An automatic detection of the ROI using Otsu thresholding in nonlinear difference EIT imaging

A. K. Khambampati, D. Liu, S. K. Konki, K. Y. Kim

***Abstract*— Inverse problem of electrical impedance tomography is highly ill-posed therefore often prior information is used to have a satisfactory and stable solution. Recently, introduced non-linear differential imaging method estimates the initial and difference in conductivities simultaneously and is efficient in handling modeling errors. The non-linear parameterization of conductivity enables to use different regularization schemes for background and region of interest (ROI). Identifying the ROI without any prior information can be beneficial in improving the reconstruction performance. Therefore, in this paper, automatic detection of ROI is introduced using Otsu thresholding method and is then used with non-linear differential imaging. The proposed non-linear differential imaging with Otsu method (NDIWO) considers different regularization methods, i.e. total variational approach with ROI and smoothness prior with background regions during reconstruction. Numerical and experimental studies are performed to test NDIWO method for two- phase flow and thorax imaging and the performance is compared with absolute and linear difference imaging. The results indicate that the proposed NDIWO method has improved reconstruction performance compared to conventional absolute and linear difference imaging.**

***Index Terms*— Difference imaging, electrical impedance tomography, inverse problem, region of interest, Otsu method**

I. Introduction

Estimation or identifying region boundaries is often done in many medical and process tomography applications for monitoring the process. Electrical impedance tomography (EIT) is a non invasive imaging technique that can provide cross sectional image about the internal distribution of an object. Moreover, EIT has high temporal resolution characteristics therefore it is suitable to monitor rapid changes in multiphase flow and thorax imaging. In EIT, electrical currents are applied through the electrodes attached on the circumference of the process pipe and the resulting voltages due to the presence of the medium inside are measured. And using a proper reconstruction algorithm, the internal distribution is reconstructed. EIT has been applied to several fields such as geophysics, medical, industrial process monitoring, non destructive testing etc [1].

Process tomography applications involving multiphase flow are one of the major studies that are studied currently. For example, in nuclear industry, we often come across steam-water two-phase in water reactors, in crude oil extracting and transportation, air-water-oil three phase flow is observed in wells, in chemical engineering process plants with reactors and bubble columns etc [2]. In the all these applications, monitoring of flow process is essential for efficacy and safety of process plant. Multiphase on the other hand has complex behavior and poses great challenge in designing measurement techniques [3]. There have been few measurement methods developed to investigate multiphase flows but none of them are practically applicable or acceptable universally. Flow patterns are generally obtained by visual observations through high-speed camera for transparent vessels. For situations where the vessel or pipe is not transparent void fraction sensors using electrical impedance or radiation based techniques are used [4]. Several imaging methods are employed to process tomography that include X-ray, gamma densitometry, ultrasound tomography, positron emission tomography, magnetic induction tomography and electrical tomography. A general methodology of all the above methods is to measure the signal from the sensors that are placed over the surface of the vessel or pipe and then compute the internal distribution or velocity profile with the use of a suitable reconstruction algorithm [5]. The applicability of process tomography imaging for the investigation of multiphase flow has been reported in papers [6-12].

In medical imaging, it is necessary to obtain internal distribution of the body that has different resistivity value of each tissue for diagnosis. EIT can be applied to locate malicious anomalies such as breast cancer cells [13] and also various physiological phenomenon can be studied, for example, cardiac, pulmonary and respiratory functions[14-16]. EIT for human thorax monitoring is an important clinical application and it is mainly used to continuously monitor acute respiratory distress syndrome (ARDS), lung perfusion, lung ventilation, lung fluid content, cardiac output right at the bedside.

The EIT inverse problem of reconstructing internal distribution is highly ill-posed due to the nonlinear relation between computed voltages and resistivity distribution [17-19]. Therefore, even a small change in voltages can result in

A. K. Khambampati is with BK21+ Clean Energy Convergence and Integration Center for Human Resources, Jeju National University, Jeju 63243, South Korea. D. Liu is with CAS Key Laboratory of Microscale Magnetic Resonance and Department of Modern Physics, University of Science and Technology of China (USTC), Hefei 230026, China, S. K. Konki is with Faculty of Applied Energy Systems, Major of Electronic Engineering, Jeju National university, Jeju 63243 South Korea. K. Y. Kim is with Department of Electronic Engineering, Jeju National University, Jeju 63243 South Korea (corresponding author e-mail: kyungyk@jejunu.ac.kr).

Manuscript received August xx, 2017; revised November xx, 2017. This work was supported by Mid-career Researcher Program through the National Research Foundation of Korea (NRF) grant funded by the Korea government (MSIP) (No. NRF-2017R1A2B4002224).

relatively large variation in estimated resistivities. To circumvent the ill-posedness often regularization methods are used to stabilize the solution. Moreover, prior information is used to improve the spatial resolution further [1]. The problem of reconstructing the resistivity distribution is done by minimizing the regularized cost function. The EIT imaging is accomplished by applying two approaches namely absolute and difference imaging. Absolute imaging is a conventional method that involves solving the nonlinear inverse problem for conductivity distribution. But, in many applications, the change in internal distribution between two measurements is of main interest which is termed as difference imaging. That is, the conductivity change is estimated based on the difference in voltage data of before and after the change. While the absolute imaging gives us the quantitative information the difference imaging gives qualitative information.

In difference imaging, the relationship between internal resistivity distribution and measured voltage is considered to be linear. The linearization is done with respect to prior defined conductivity and the inverse solution is obtained by solving the regularized linear least squares problem. Difference imaging methods often considers linearizing the model except in few cases such as D-bar method. Linearized difference imaging (LDI) is widely used as it is non iterative and the computational time for image reconstruction is fast therefore it can be applicable for real-time monitoring. Moreover, modeling errors are compensated to some extent due to subtraction of voltage measurements collected before and after the change from the same domain. However, the linearization of forward model is only valid for small changes from initial conductivity distribution. Thus, LDI method may be inadequate in situations containing high contrast and inhomogeneous conditions such as multiphase flow. Moreover, the performance of the LDI method depends on the linearization point which is often considered as initial distribution. In many situations, the initial state is approximated by a constant value using least squares fit to voltage data corresponding to initial distribution. If the initial distribution is not known or if the initial or final distribution is very inhomogeneous as in case of multiphase flow then LDI reconstructions may have low spatial resolution with artifacts.

Modeling errors in EIT are due to unknown shape of outer boundary, imprecise location of electrodes, unknown contact impedances of electrodes [20-21]. If the modeling errors are not taken care off, then the conventional nonlinear absolute imaging can have erroneous solution. One way to circumvent the modeling errors is by treating them as an additional state parameter and estimate them simultaneously with conductivity distribution. However, the above approach can handle only small changes in conductivity and electrode movement. Another approach is to compute the absolute reconstructions of measurements from data sets corresponding to before and after change and then subtracting the reconstructions. In this way to some extent the artifacts present in conventional absolute imaging are removed. For multiphase flow applications where quantitative information is desired, it is preferred to model the nonlinear absolute imaging for handing the uncertainties and improve the spatial resolution. Recently introduced nonlinear difference imaging estimates simultaneously both the initial distribution and change in distribution from the measurements collected before and after the change [22]. The conductivity/resistivity after the change is parameterized as a linear combination of initial distribution and change in the distribution. This parameterization restricts the change in distribution to a sub-domain or region of interest (ROI) inside the object. The parameterization is helpful in restricting the conductivity change to ROI if the changes that occur in the computational domain take place in known region. And another major advantage is that different type of regularization can be employed to initial and change in resistivity regions which can further improve the reconstruction performance. Moreover, nonlinear difference imaging does not linearize the measurement model therefore it can handle multiphase conditions with high contrast and inhomogeneous background. In [23], robustness of nonlinear difference imaging is studied for modeling errors. The results in [23] show that the nonlinear imaging has better reconstruction performance as compared to linear difference imaging and conventional absolute imaging in the presence of modeling errors that include unknown electrode contact impedance, inaccurate knowledge of electrode position, unknown outer domain boundary and domain truncation. In the above studies it is assumed that ROI is known *a priori* and the known ROI is used for parameterization of conductivity. In real situations, ROI is not known a priori and in multiphase flow the flow distribution is very transient therefore it is difficult to select the ROI region. It is very useful if there is a way to determine the ROI automatically and then use with nonlinear difference imaging.

In this paper, an automatic detection of ROI is presented for multiphase flow imaging. The ROI is determined using Otsu thresholding method [24]. Using Otsu method it is possible to classify the regions as target and background based on the first iteration estimate of Gauss Newton method [25-26]. The target region is considered as ROI and is used in nonlinear difference imaging. The nonlinear reconstruction problem of determining the time varying distribution is done by appending the measurements collected for distributions corresponding to before and after the change. The ROI is selected based on Otsu method and separate regularization functional is used for background and target containing in ROI. Numerical simulations and phantom experiments pertaining to multiphase flow are performed with high contrast conditions. The reconstructions using proposed nonlinear difference imaging with Otsu method is compared against conventional absolute imaging and traditional linear difference method.

II. EIT IMAGE RECONSTRUCTION

2.1. Forward problem

In EIT, surface electrodes e_l ($l = 1,2,\cdots,L,$) are placed on the circumference $\partial\Omega$ of the process pipe. Time varying electrical currents I_l ($l = 1,2,\cdots,L$) are injected into the domain through the boundary electrodes that has electrical resistivity distribution $\rho(x)$ within the domain boundary, then the resulting electrical potential $u(x)$ on the Ω is calculated by

using the governing equation, which can be derived through the Maxwell equations [1]

$$\nabla \cdot \left(\frac{1}{\rho(x)} \nabla u(x) \right) = 0, \quad x \in \Omega \tag{1}$$

The above Laplace equation can be solved for potential distribution by applying suitable boundary conditions. The electrode model that is used to model the EIT measurements is based on complete electrode model (CEM). CEM is more accurate and realistic model that is used to model the EIT measurements. The boundary conditions based on CEM are given by [27]

$$u(x) + z_l \frac{1}{\rho(x)} \frac{\partial u(x)}{\partial \mathbf{n}} = V_l, \quad x \in e_l, \; l = 1,2,\cdots,L, \tag{2}$$

$$\int_{e_l} \frac{1}{\rho(x)} \frac{\partial u(x)}{\partial \mathbf{n}} dS = I_l, \quad x \in e_l, \; l = 1,2,\cdots,L, \tag{3}$$

$$\frac{1}{\rho(x)} \frac{\partial u(x)}{\partial \mathbf{n}} = 0, \; x \in \partial\Omega \setminus \bigcup_{l=1}^{L} e_l \tag{4}$$

where L is the number of electrodes on boundary, z_l is the effective contact impedance between lth electrode and surface of the pipe, V_l is the measured electrical potentials on the lth surface electrode, and I_l is the applied alternating current applied through the lth electrode. In addition to the electrode model, the following Kirchhoff's rules on the measured potentials and the injected currents should guarantee the existence and uniqueness of the solution [27]

$$\sum_{l=1}^{L} I_l = 0, \qquad \sum_{l=1}^{L} V_l = 0 \tag{5}$$

The solution using the governing equation (1) and the boundary conditions (2-5) is obtained numerically and the solution is based on finite element (FE) approximation. The domain is discretized into small triangular elements each having a constant resistivity distribution. In FE formulation, the potential distribution and resistivity inside the domain are approximated as

$$\rho \approx \rho^h(x) = \sum_{i=1}^{N_E} \rho_i \phi_i(x) \tag{6}$$

$$u \approx u^h(x) = \sum_{i=1}^{N} \alpha_i \varphi_i(x) \tag{7}$$

where N_E and N are the number of elements and nodes in finite element mesh, ϕ, φ_i are the first-order nodal basis functions for resistivity and potential, respectively. α_i are the nodal voltages that are to be determined . The voltages on the electrodes is approximated as

$$U^h = \sum_{j=1}^{L-1} \beta_j \mathbf{n}_j \tag{8}$$

where the bases for the measurement are $n_1=(1,-1,0,\ldots\ldots0)^T$, $n_2=(1,0,-1,0,\ldots\ldots0)^T \in \Re^L$, etc. Here, β_j are the boundary voltages which are the unknowns to be determined. From (5-8), the FEM solution to the CEM model (2-5) can be represented as a set of linear equations

$$\mathbf{Ab} = \tilde{\mathbf{I}} \tag{9}$$

where A is the stiffness matrix and the solution vector b and data vector $\tilde{\mathbf{I}}$ are of the form

$$\mathbf{b} = \begin{pmatrix} \boldsymbol{\alpha} \\ \boldsymbol{\beta} \end{pmatrix} \tag{10}$$

$$\tilde{\mathbf{I}} = \begin{pmatrix} \mathbf{0} \\ \boldsymbol{\zeta} \end{pmatrix} \tag{11}$$

where $\boldsymbol{\alpha} \in \Re^N$, $\boldsymbol{\beta} \in \Re^{(L-1)}$ are the nodal and boundary voltages and $\mathbf{0} \in \Re^N$, $\zeta = (I_1 - I_2, I_1 - I_3, .., I_1 - I_L)^T = N^T \hat{\mathrm{I}} \in \Re^{(L-1)}$ is the reduced current vector. The discretized forward mapping with FEM is represented as $U(\rho)$. For more details of FEM approximation using CEM see [28]. Assuming the measurements are associated with additive Gaussian noise and with FEM approximation, the observation model has the form

$$V = U(\rho) + e \tag{12}$$

where $V \in \Re^M$ is the vector that includes all the measured voltage potentials. The number of measurements $M = mN_{CP}$, where N_{CP} is the number of current injections used and m are number of measured potentials recorded with each current pattern. The Gaussian noise $e \sim \mathrm{N}(e^*, \Gamma_e)$ has mean e^* and covariance Γ_e that are determined experimentally. Based on the above measurement model, various inverse methods can be obtained that are discussed in the next section.

2.2. Inverse problem

In EIT, the inverse problem is to estimate the resistivity distribution from the measured voltages and known applied injected currents. The resistivity is determined by minimizing the cost function such that the difference between the measured and computed voltages is minimized. EIT image reconstruction types can be categorized mainly as absolute and difference imaging techniques [17,22].

2.2.1 Absolute imaging

In absolute imaging, from the measured set of voltage measurements V within which the target is assumed to be stationary, the resistivity is reconstructed. Most of the inverse approaches of EIT are formulated using nonlinear least squares approach employing regularization. The resistivity is achieved by minimizing the cost function which is of the form

$$\hat{\rho} = \arg\min \left\{ L_e \left\| V - U(\rho) \right\|^2 + R(\rho) \right\} \tag{13}$$

where L_e is the weighting matrix, $R(\rho) \geq 0$ is a regularizing penalty functional. The above cost functional is solved for resistivity distribution iteratively using Gauss Newton method. Due to the ill-posedness of the EIT inverse problem, the reconstruction problem is very sensitive to measurement noise and modeling errors. The modeling errors are caused due to inaccurate knowledge of electrode locations, contact impedance of electrodes, outer boundary of the object, truncation of computation domain etc. The modeling errors if not compensated, the reconstruction with absolute imaging will have erroneous image.

2.2.2 Linear difference imaging (LDI)

In many applications, for example, lung ventilation, it is often needed to monitor the change in resistivity with respect to time rather than the absolute value. This is termed as difference imaging. Difference imaging is done using two measurements

V_1 and V_2 recorded at different time instants t_1 and t_2 which correspond to the resistivity distribution ρ_1 and ρ_2. The resistivity change is estimated from previous or reference distribution. The observation model corresponding to the two measurements can be written as

$$V_1 = U(\rho_1) + e_1 \tag{14}$$

$$V_2 = U(\rho_2) + e_2 \tag{15}$$

where e_1, e_2 are measurement noise associated with measurements. In LDI the observation model are linearized with respect to nominal distribution as follows

$$V_i = U(\rho_o) + \mathrm{J}(\rho_i - \rho_o) + e_i,\ i = 1,2 \tag{16}$$

where J is the Jacobian matrix evaluated at ρ_o. The linearized models upon subtracting results in a new observation model based on difference data as

$$\delta V = \mathrm{J}\delta\rho + \delta e \tag{17}$$

The goal is to estimate the resistivity change based on the difference voltage data which can be represented as a minimization problem

$$\widehat{\delta\rho} = \arg\min\left\{L_{\delta e}\left\|\delta V - \mathrm{J}\delta\rho\right\|^2 + R(\delta\rho)\right\} \tag{18}$$

when using difference data since both measurements are from same system therefore part of the modeling errors can be compensated. As, we are linearizing the observation model the linearity can only exists for a small change in resistivity. If the resistivity contrast is high then the linear difference imaging will produce unsatisfactory performance.

III. NONLINEAR DIFFERENCE IMAGING

Using absolute imaging, the distributions ρ_1 and ρ_2 are reconstructed from measurements V_1 and V_2 by solving separately and the change in resistivity $\delta\rho$ is then obtained upon subtracting the estimated distributions $\widehat{\rho}_1$ and $\widehat{\rho}_2$. In the nonlinear difference imaging, the initial $\widehat{\rho}_1$ and the change in resistivity $\delta\rho$ are reconstructed simultaneously using the measurements V_1 and V_2. Moreover, the resistivity after the change is modeled as a linear combination of the initial resistivity and the change in resistivity as

$$\rho_2 = \rho_1 + \kappa\delta\rho \tag{19}$$

where κ is the mapping operator. Using the above parameterization in measurement V_2, it can be written as

$$V_2 = U(\rho_1 + \kappa\delta\rho) + e_2 \tag{20}$$

Now augmenting the measurements V_1 and V_2 into single vector we have the new observation model for nonlinear difference imaging as follows [18-19]

$$\overline{V} = \overline{U}(\overline{\rho}) + \overline{e} \tag{21}$$

where $\overline{\rho} = \begin{bmatrix}\rho_1 \\ \delta\rho\end{bmatrix}$ is the initial and change in resistivity to be estimated and it is obtained by minimizing the cost functional

$$\widehat{\overline{\rho}} = \arg\min\left\{L_e\left\|\overline{V} - \overline{U}(\overline{\rho})\right\|^2 + R(\overline{\rho})\right\} \tag{22}$$

The change resistivity is restricted to a region of interest ROI then the compound regularization functional $R(\overline{\rho})$ is represented as

$$R(\overline{\rho}) = R(\rho_1) + R(\delta\rho_{ROI}) \tag{23}$$

where $\delta\rho_{ROI}$ is resistivity change within the region of interest. ROI is difficult to determine for two-phase flow conditions as the flow is very transient. If ROI can be determined automatically then it can be used in the above parameterization and different type of regularized methods can be used with initial and resistivity change thus it can improve the reconstruction performance.

IV. DETERMINING ROI USING OTSU METHOD:

To determine the ROI automatically we employ Otsu thresholding method. An adaptive threshold is determined by Otsu method by minimizing the between class variance with a comprehensive search from a resistivity histogram which can be used to separate the background area from the resistivity distribution with anomalies [24-26]. Let the image to be reconstructed is represented as L gray levels $\{1,2,\cdots,t,\cdots,L\}$, and is separated into two different classes A and B by a threshold at level t. Here, A denotes the elements having index from 1 to t, and B denotes the elements with index $t+1$ to L. If suppose the number of elements at a given index level j is represented by o_j then the total number of elements N will be $N = o_1 + o_2 + \ldots + o_L$. Otsu thresholding method determines the optimal threshold that minimizes the within-class variance, or equivalently maximizes the between-class variance. The with-in class and between class variance are described as [24]

$$\rho^2_{within}(t) = \omega_A\rho^2_A + \omega_B\rho^2_B, \tag{24}$$

$$\begin{aligned}\rho^2_{between} &= \rho^2_T - \rho^2_{within} \\ &= \omega_A(\mu_A - \mu_T)^2 + \omega_B(\mu_B - \mu_T)^2 = \frac{[\mu_T\omega(t) - \mu(t)]^2}{\omega(t)[1-\omega(t)]},\end{aligned} \tag{25}$$

where ω_A, ω_B the probabilities of class occurrence, μ_A, μ_B the class mean levels that are defined as

$$\omega_A = \sum_{j=1}^{t} p_j = \omega(t),\ \omega_B = \sum_{j=t+1}^{L} p_j = 1 - \omega_A = 1 - \omega(t), \tag{26}$$

$$\mu_A = \frac{1}{\omega_A}\sum_{j=1}^{t} jp_j = \frac{\mu(t)}{\omega(t)},\ \mu_B = \frac{1}{\omega_B}\sum_{j=t+1}^{L} jp_j = \frac{\mu_T - \mu(t)}{1-\omega(t)}, \tag{27}$$

$$\mu_T \equiv \mu(L) = \sum_{j=1}^{L} jp_j \tag{28}$$

From the above computations, the optimal threshold t^* can be computed using

$$t^* = \arg\max_{1\le t<L} \rho^2_B(t). \tag{29}$$

Find index vectors d_b and d_a for the background and anomaly regions, respectively using threshold as

$$(d_b, d_a) = \text{find\_index}(\tilde{\rho} \le t^*) \quad \text{if } \rho_{\text{bac}} < \rho_{\text{tar}} \tag{30}$$

$$(d_b, d_a) = \text{find\_index}(\tilde{\rho} \ge t^*) \quad \text{if } \rho_{\text{bac}} > \rho_{\text{tar}} \tag{31}$$

where ρ_{bac} and ρ_{tar} denote the background and the target resistivity values, respectively, which could be approximately known in two-phase flows. The index vectors d_a is used as ROI

in nonlinear difference method in resistivity parameterization.

V. RESULTS

In this section, the viability of the proposed NDIWO method is tested with numerical and experimental studies. The proposed method is applied to two-phase flow and thorax imaging. The computational domain consists of regions having resistive targets visualized to be voids or organs enclosed in a homogeneous background. The proposed NDIWO method is compared against conventional absolute imaging (ABI) and linear difference imaging (LDI). The estimates for NDIWO, ABI and LDI are computed as follows

Absolute imaging (ABI): The ABI estimates are obtained by solving

$$\hat{\rho}_i = \arg\min\left\{\left\|L_e(V-U(\rho_i))\right\|^2 + \alpha_s\left\|L_\rho(\rho_i-\rho^*)\right\|^2\right\}, i=1,2 \quad (32)$$

where $\hat{\rho}_1$, $\hat{\rho}_2$ are the estimates of initial and final distribution, ρ^* is the prior information of resistivity distribution, α_s is the regularization parameter and $L_\rho{}^T L_\rho = \Gamma_\rho{}^{-1}$, Γ_ρ is covariance matrix considering smoothness prior. The estimated change in resistivity is obtained as $\widehat{\delta\rho} = \hat{\rho}_2 - \hat{\rho}_1$. A general choice for regularization matrix Γ_ρ that is used with smoothness prior is the difference-type matrix [29-30]. The whole object domain is discretized with triangular elements and the resistivity distribution is estimated in element basis. In this case, the gradient of resistivity of the i th element can be approximated as the difference in the resistivity of i th element and the neighboring elements that share a common edge. The i th row of difference regularization matrix Γ_ρ can be expressed as follows [30]

$$\Gamma_{\rho_i} = [0,\cdots,0,-1,0,\cdots,0,-1,0,\cdots,0,3,0,\cdots,0,-1,0,\cdots,0], \quad (33)$$

here, weight of 3 is assigned to the i th column and -1s are assigned to the columns corresponding to the neighboring elements that share with i th element.

Nonlinear differential imaging with Otsu method (NDIWO): The estimates of NDIWO are determined by solving the below minimization equation

$$\widehat{\widehat{\rho}} = \arg\min\left\{\left\|L_e\left\|\overline{V}-\overline{U}(\overline{\rho})\right\|^2 + \alpha_s\left\|L_{\rho_1}(\rho_1-\rho^*)\right\|^2 + \alpha_{TV}\mathrm{TV}(\delta\rho_{\mathrm{ROI}})\right\}\right. \quad (34)$$

where the estimate $\widehat{\widehat{\rho}}$ is $\widehat{\widehat{\rho}} = [\rho_1{}^T, \delta\rho_{\mathrm{ROI}}{}^T]^T$, α_{TV} is the weighting parameter and TV is total variational functional which is defined as

$$\mathrm{TV}(\rho) = \sum_{k=1}^{N_E} |e_k| \sqrt{\left\|(\nabla\rho)\big|_{e_k}\right\|^2 + \beta} \quad (35)$$

here N_E is number of finite element meshes, $(\nabla\rho)\big|_{e_k}$ is the gradient of ρ at element e_k and β is a parameter which ensures the function is differentiable. $L_{\rho_1}{}^T L_{\rho_1} = \Gamma_{\rho_1}{}^{-1}$, Γ_{ρ_1} is covariance matrix considering smoothness prior which is defined in (33). Selecting prior parameters especially α_{TV} is important in order to have good reconstruction performance. For situations when there is no prior information available about range of conductivity values inside the object domain, the prior parameter alpha is normally selected based on quality of reconstructed images using trial and error approach or by considering alpha as state variable and then estimate it along with conductivity values. Determining optimal prior parameters automatically is beneficial and is possible in cases where the prior information is available on the range of conductivities within the object to be imaged [31]. In situations when the maximum or minimum conductivity within in the object domain is known then alpha can be determined as follows [31]

$$g_{\max} = \frac{\sigma_{\max} - \sigma_{\min}}{d} \quad (36)$$

$$\alpha_{TV} = -\frac{\ln\left(1-\frac{p}{100}\right)}{g_{\max}} \quad (37)$$

where d is the mean edge of mesh element, p is the probability for which the gradient norm values within the domain are below or equal to $g_{\max}$. After the 1st iteration of GN, Otsu method is used to classify the regions and the target regions are considered as region of interest (ROI). Different regularization methods are used for background and target regions i.e. smoothness prior is used with background region and the ROI is penalized with TV regularization and is termed as NDIWO-TV method. If smoothness prior is used for both background and ROI regions in nonlinear approach we term the method as NDIWO-SP.

Linear difference imaging (LDI): The estimate $\widehat{\delta\rho}$ is computed by solving

$$\widehat{\delta\rho} = \arg\min\left\{L_{\delta e}\left\|\delta V - \mathrm{J}\delta\rho\right\|^2 + \alpha_s\left\|L_{\delta\rho}\delta\rho\right\|^2\right\} \quad (38)$$

here $L_{\delta\rho}{}^T L_{\delta\rho} = \Gamma_{\delta\rho}^{-1}$ is covariance matrix which is constructed based on smoothness prior using (33).

The above estimates for ABI, NDIWO, and LDI are computed using optimization algorithm based on Gauss Newton method. As a performance metric, root mean square error (RMSE) of estimated resistivity, correlation coefficient (CC), ratio of coverage area (RCR) and relative contrast (RCo) are computed for the estimated change in resistivity and are defined as

$$\mathrm{RMSE} = \frac{\left\|\delta\rho - \widehat{\delta\rho}\right\|}{\left\|\delta\rho\right\|}, \quad (39)$$

$$\mathrm{CC} = \frac{\sum_{i=1}^{N}[(\delta\rho_i - \overline{\delta\rho})(\widehat{\delta\rho}_i - \overline{\widehat{\delta\rho}})]}{\sqrt{\sum_{i=1}^{N}(\delta\rho_i - \overline{\delta\rho})^2 \sum_{i=1}^{N}(\widehat{\delta\rho}_i - \overline{\widehat{\delta\rho}})^2}}, \quad (40)$$

where $\delta\rho$, $\widehat{\delta\rho}$ are true and estimated change in resistivity, respectively. Also, $\overline{\delta\rho}$, $\overline{\widehat{\delta\rho}}$ are the mean values of $\delta\rho$ and

$\widehat{\delta\rho}$, respectively. It should be noted that the smaller RMSE and bigger CC values correspond to better reconstruction performance. ABI and NDIWO methods are iterative whereas LDI is non-iterative. Therefore for comparison of RMSE and CC we have used mean RMSE and CC values. RCR denotes how good the inclusions are reconstructed and is defined as [23]

$$\mathrm{RCR} = \frac{\mathrm{CR}}{\mathrm{CR}_{\mathrm{True}}} \tag{41}$$

where CR is ratio of inclusion area to total area of domain, i.e.

$$\mathrm{CR} = \frac{\text{Inclusion area}}{\text{Domain area}} \tag{42}$$

To estimate the area of estimated inclusion, we have used half the maximum value of the estimates $\widehat{\delta\rho}$ as the threshold to determine the inclusion area. Further, the contrast of the resistivity is measured by computing the maximum/minimum of reconstructed change, i.e.

$$\mathrm{RCo} = \frac{\max\left|\delta\hat{\rho}\right|}{\max\left|\delta\rho_{\mathrm{True}}\right|} \tag{43}$$

The values of RCR and RCo equal to 1 would indicate the exact match of change in resistivity of reconstructed and true distribution. At the same time, a value greater or less than 1 would indicate over estimation and under estimation, respectively.

5.1. Simulation studies for two phase flow monitoring

Numerical experiments are conducted for two-phase flow using a circular industrial process pipe of radius 4 cm with 32 electrodes of width 0.6 cm are attached across the outer periphery of pipe. Finite element mesh for the above geometry and electrode configuration is used for numerical simulation. Fine mesh containing 3984 triangular elements is used for generating the true data and coarse mesh with 996 elements is used for inverse computation of resistivity. Adjacent current method with magnitude of 1 mA is used as a current injection. Two test cases are considered where in case 1 is with two relatively small circular targets visualized as bubbles. Initial distribution ρ_1 of Case 1 has a small circular inclusion with resistivity 5000 Ω-cm appearing at the south west side of flow domain containing background liquid that has resistivity 300 Ω-cm. Final distribution ρ_2 after the change in distribution has another circular inclusion of resistivity 10000 Ω-cm appearing at north east corner. The true data distribution for case 1 with small target is given in Figure 1(top row). The true voltages are generated for initial, final distributions and 1 percent random Gaussian noise is added to the generated voltages to take into account the measurement noise and numerical errors. In case 2, we study the effect of smoothly varying objects in flow field. The initial distribution ρ_1 for case 2 has a circular inclusion with smoothed resistivity profile enclosed within homogeneous background liquid that has resistivity 150 Ω-cm. The final resistivity distribution ρ_2 has an elliptic inclusion with smoothed resistivity profile that additionally appears in north side of flow domain.

5.2. Simulation studies for thorax imaging

Numerical simulations for thorax imaging are performed using chest shaped finite element mesh. The FEM mesh for thorax imaging is modeled based on the available CT image of chest. The FEM mesh has sixteen electrodes placed on the circumference of chest for current injection and voltage measurement. Two different meshes are used in forward and inverse computation in order to avoid inverse crime. Fine mesh (Mesh 2) with 3028 elements is used to generate true voltages and coarse mesh (Mesh 1) with 2216 elements is used for estimating internal resistivity distribution. True voltages are generated with clinical resistivity values of thorax for background, heart and lungs, respectively. Moreover, as a current injection method, adjacent type is considered where neighboring electrodes are used for current injection.

Thorax imaging is studied as Case 3 in numerical simulations. Lung ventilation is considered as an application where the during the respiration process the resistivity of lungs changes due to the intake of air. Initial distribution ρ_1 is simulated with thorax resistivity of background, heart and lungs assumed to be 495 Ωcm, 207 Ωcm and 645 Ωcm, respectively. After time t, due to respiration, the lung resistivity is changed to 1400 Ωcm and the final distribution is obtained by considering thorax resistivity of background, heart and lungs assumed to be 495 Ωcm, 207 Ωcm and 1400 Ωcm, respectively.

5.3 Simulation results

The true distributions along with estimated resistivity distribution for test cases 1-3 are given in Figures 1-3. In figures 1-3, top row has the true distribution for initial distribution (ρ_1), distribution after change (ρ_2) and the change in the distribution ($\delta\rho$). While the second, third, fourth and fifth rows are the estimated results using ABI, NDIWO-SP, NDIWO-TV and LDI methods. The estimates of nonlinear approach employing smoothness prior in both background and ROI region (NDIWO-SP) and nonlinear approach employing smoothness prior for background and TV regularization for ROI region (NDIWO-TV) are compared for all cases. This comparison can give us an idea about the characteristics of nonlinear approach. The estimates of initial, final distribution and change in distribution are shown in columns 1-3. To evaluate the reconstruction performance RMSE and CC are computed and shown in Table 1. To quantify the results further, the target size and relative resistivity contrast is computed for estimates of change in resistivity as RCR and RCo. The RCR and RCo value for the test cases 1-3 are shown in Table 2. Simulation parameters that are used for reconstruction are given in Table 3. The average mesh size d for case 1-2 is 0.05 and case 3 is 0.31. When we compute the g_{max} for case1-2 using eq. (36) the value is 0.0655 and for case 3 is 0.0133. Hence alpha α_{TV} for case 3 is considered 5 times less than case 1-2. The prior values that are used in numerical and experiment cases is given below in table 3 and the reconstruction results using those prior parameters are shown in Figs 1-4.

Figure 1 has the reconstruction results for case 1 with sharply varying small targets. The results with the absolute estimates using ABI, NDIWO approach and the difference estimate of

LDI are shown in Figure 1. As can be noticed from figure1, all the estimates were able to locate inclusions in initial, final and change in resistivity distributions. However, the estimate with proposed NDIWO has better resolution as compared to other estimates with uniform background. It is found that size of inclusion is over estimated with all methods but the size of inclusion with NDIWO methods has better estimation as noticed from the computed RCR values in Table 2. The estimated resistivity contrast is also less with all approaches. The root mean square of estimated change in resistivity and correlation coefficient for case 1 are shown in Table 1. In case 1 of Table 1, it is seen that RMSE of estimated change in conductivity of all the estimates is similar while the CC value of proposed NDIWO methods has higher value compared to ABI and LDI methods. The performance of NDIWO-SP is found to be visually similar with NDIWO-TV. However, when we compare the values of RMSE, CC, RCR and RCo it can be said that NDIWO-TV has slightly better performance than NDIWO-SP.

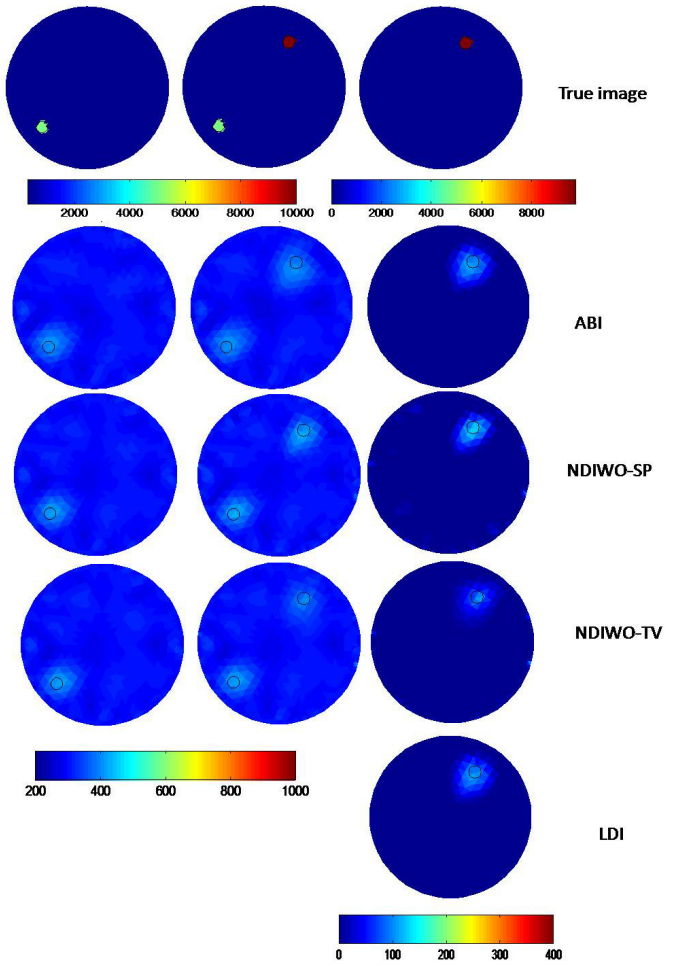

Figure 1. Numerical results for case 1 to estimate region boundaries in two-phase flow. Top row contains true resistivity data and second, third and fourth row are the estimated resistivity using absolute (ABI), nonlinear difference imaging with Otsu method employing smoothness prior (NDIWO-SP) and TV regularization (NDIWO-TV) and linear difference imaging (LDI).

Figure 2 has the result for test case 2 with smoothly varying inclusions located in flow domain. The initial distribution of inhomogeneous background comprising of inclusion located at south west side and then the final distribution has another inclusion that appears in north east side. Based on the estimates for case 2, it can be noticed that the inclusions for the change in the distribution are detected by NDIWO-SP, NDIWO-TV, ABI and LDI methods. Although, inclusion is detected using ABI, there can be seen many artifacts in estimated background region of change in resistivity distribution. But the estimates of NDIWO have estimated the shape and size of inclusion with a better accuracy. From Table1-2, from the computed RMSE, CC, RCo values and the size estimate (RCR), it can be found that NDIWO-SP method has better reconstruction performance. With LDI, the background region is uniform due to compensation of numerical errors with difference imaging but the estimates of target size is bigger and the estimated contrast is low compared to the true value (Table 2).

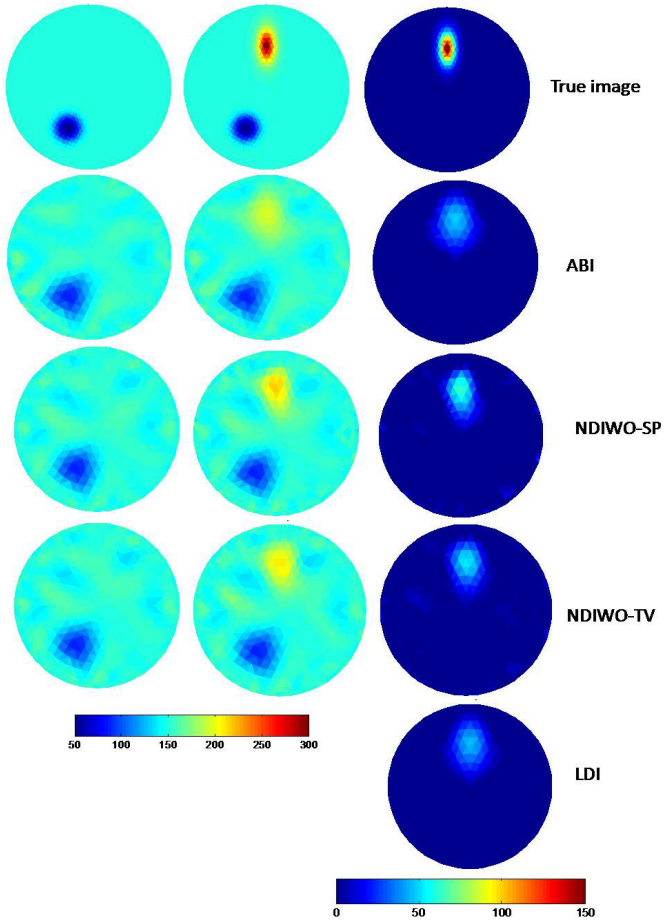

Figure 2. Numerical results for case 2 with smoothly varying targets to estimate region boundaries in two-phase flow. Top row contains true resistivity data and second, third and fourth row are the estimated resistivity using absolute (ABI), nonlinear difference imaging with Otsu method employing smoothness prior (NDIWO-SP) and TV regularization (NDIWO-TV) and linear difference imaging (LDI).

The reconstruction results for thorax imaging (case 3) are shown in Figure 3. The estimates of nonlinear approach NDIWO are found to have better resolution and have recovered

This article has been accepted for publication in a future issue of this journal, but has not been fully edited. Content may change prior to final publication. Citation information: DOI 10.1109/JSEN.2018.2828312, IEEE Sensors Journal

the shape and size of lungs with better accuracy as compared to ABI and LDI. Among the nonlinear estimates, NDIWO-TV has best reconstruction performance as can be seen clearly by visualization and from the computed RMSE and correlation values (Table 1). Also, the size estimation and the estimated resistivity contrast are better with NDIWO-TV method (Table 2). The estimates of NDIWO-SP have uniform background and lungs estimated with good accuracy. However, it has overestimated the lungs resistivity thereby having lower computed RCR value. The reconstructions of ABI have non uniform background and have overestimated the lung resistivity while the size of lungs is underestimated as compared to true size. The LDI estimate is found to have uniform background but as with ABI the size of inclusion is less than the true value (Table 2).

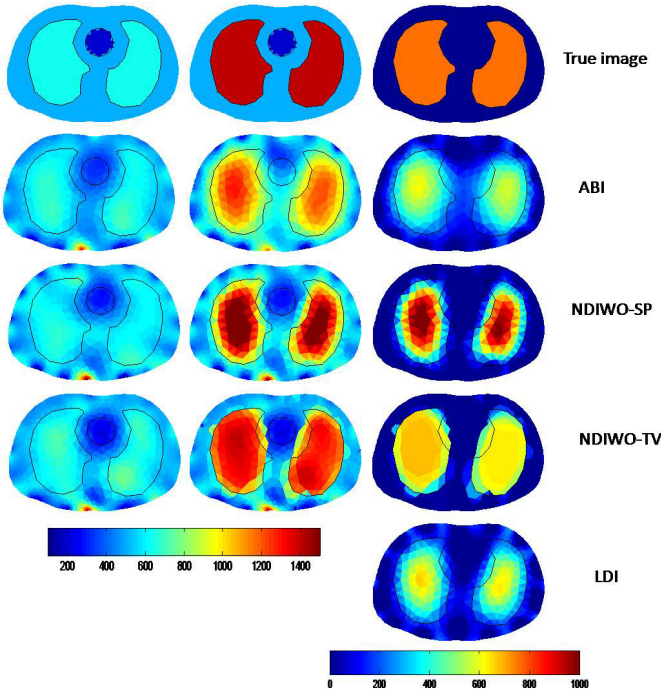

Figure 3. Numerical results for case 3 with thorax imaging. Top row contains true resistivity and second, third and fourth row are the estimated resistivity using absolute (ABI), nonlinear difference imaging with Otsu method employing smoothness prior (NDIWO-SP) and TV regularization (NDIWO-TV) and linear difference imaging (LDI).

Table 1. RMSE conductivity and correlation coefficient of estimated resistivity change for numerical simulations

Performance metric	Case 1		Case 2		Case 3	
	RMSE	CC	RMSE	CC	RMSE	CC
NDIWO-TV	0.9916	0.4312	0.5977	0.8251	0.5818	0.8318
NDIWO-SP	0.9886	0.4260	0.5635	0.8238	0.6273	0.8001
ABI	0.9898	0.4211	0.6083	0.8044	0.6722	0.5505
LDI	0.9902	0.4299	0.6103	0.8158	0.7041	0.6716

Table 2. Relative size coverage ratio and relative contrast of estimated resistivity change for numerical simulations

Performance metric	Case 1		Case 2		Case 3	
	RCR	RCo	RCR	RCo	RCR	RCo
NDIWO-TV	2.6186	0.0112	3.6293	0.3535	1.0362	0.8944
NDIWO-SP	4.7792	0.0131	3.3477	0.4180	0.5838	1.3997
ABI	6.1619	0.0116	5.2760	0.3139	0.8442	0.8086
LDI	5.6744	0.0111	5.0422	0.2993	0.6419	0.8769

Table 3. Parameters used in reconstruction for numerical and experimental studies

	Simulated data			Experiment data
	Case 1	Case 2	Case 3	Case 1
α_s	0.00005	0.00005	0.001	0.0005
α_{TV}	0.05	0.05	0.05	0.05
β	0.0001	0.0001	0.0001	0.0001

5.3 Experimental studies

The applicability of proposed method is further evaluated with experiment studies. The experiment is carried out using a cylindrical tank of diameter 28cm with sixteen electrodes (width 2.5cm, height 7cm) placed equally in inner side of the tank (Figure 4, top row). The experimental tank is filled with saline solution and plastic objects with circular and triangular shape are visualized as inclusions that form the in-homogeneities. A plastic rod placed in the tank containing saline solution is considered as the initial state to form the inhomogeneous distribution. A plastic triangular prism was later placed in tank to consider the final state with resistivity change. The targets considered are vertically symmetric and the saline solution is filled until the height of electrode hence 2D model is sufficient in modelling measurements.

The measurements obtained for this study are from the KIT4 measurement system developed in Department of Applied physics, University of eastern Finland [32]. For more information about the experiment setup see [32]. Current with low frequency of 1 kHz and magnitude 1 mA is applied across the pair electrodes. That is, one electrode is fixed as sink electrode and as a pair, one of remaining 15 electrodes are considered and the corresponding excited potential on 15 electrodes is measured against sink or reference electrode. Four sink electrodes are considered {1,5,9,13} and the process is repeated to have a total of 54 current injections avoiding the repetition of same current patterns. Based on this measurement strategy we have 810 voltage readings. Two different experiment data are measured corresponding to initial distribution ρ_1 with circular plastic cylindrical rod of diameter 6.2 cm enclosed in saline solution and final distribution ρ_2 with plastic cylindrical rod and triangular prism in saline solution. The triangular prism used in the experiment is equilateral and has each edge that is 8.5 cm long.

To compute the contact impedances of electrode, measurements obtained from homogeneous data with saline solution is used. From the measurement data, unknown contact impedances and constant value of resistivity is computed by solving least squares problem [33]. Based on above method the estimated contact impedance is 0.025 ohm-cm. The resistivity is reconstructed using a finite element mesh of same geometry as experimental tank with 2232 nodes and 4496 elements. The results for the experiment case are shown in Figure 4. In figure 4, the top row shows the image of experiment condition for initial state ρ_1 and final state ρ_2. The reconstructed estimates $\hat{\rho}_1$, $\hat{\rho}_2$ computed from the estimates $(\hat{\rho}_1, \widehat{\delta\rho}_{\mathrm{ROI}})$ and the

change in resistivity $\widehat{\delta\rho}_{\mathrm{ROI}}$ are shown. Second row shows the absolute reconstructions of $\hat{\rho}_1$ and $\hat{\rho}_2$ and the change in resistivity $\widehat{\delta\rho}$ with ABI. Third, fourth and fifth row contains the reconstructions using NDIWO-SP, NDIWO-TV and LDI approach, respectively. The results show that NDIWO-TV has better estimation of initial, final and change in resistivity distribution. The resolution is better and the triangular prism size is recovered while shape is also close to the true shape. The estimate of NDIWO-SP has similar reconstruction performance as NDIWO-TV. With ABI, the size is over estimated as also found from the computed RCR and also the background in not uniform and has artifacts. The estimate with LDI also has over estimated the size as seen from RCR value and the background is found to have artifacts as in the case of ABI.

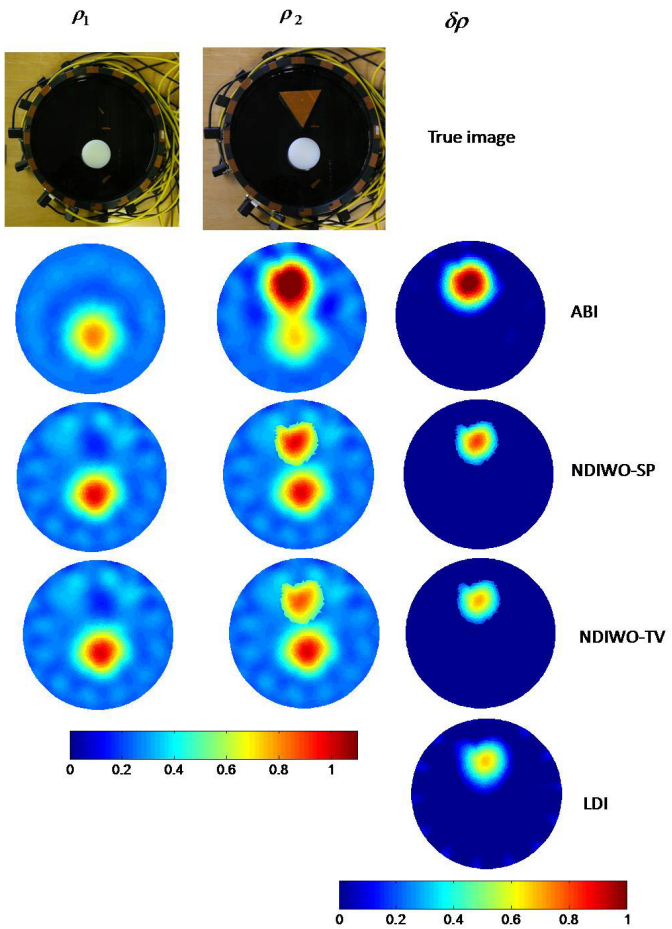

Figure 4. Experimental results for estimating two targets located in domain. Top row contains images of experiment tank with targets inside, second, third, fourth and fifth row are the estimated resistivity using ABI, NDIWO-SP, NDIWO-TV and LDI, respectively.

Table 4. Relative size coverage ratio and relative contrast of estimated resistivity change for experimental studies

Performance metric	Experiment Case 1
	RCR
NDIWO-TV	0.9894
NDIWO-SP	0.9191
ABI	1.3237
LDI	1.0998

VI. Conclusions

A nonlinear differential imaging based method is proposed to reconstruct the internal resistivity distribution using electrical impedance tomography. The resistivity is parameterized as initial and change in resistivity. The parameterization can be used to set different regularization schemes for background and target. The proposed method uses Otsu thresholding method to classify the regions as target and background after 1st iteration of Gauss Newton method and the background, ROI regions are then applied with Laplacian and TV-type regularization. Numerical and experimental studies simulating two-phase conditions are performed to evaluate the reconstruction performance. It is noticed that the proposed NDIWO method has improved spatial resolution with uniform background and has less image error and higher correlation coefficient as compared to conventional ABI and LDI. The RCR and RCo of reconstruct image of proposed method are close to the true value as compared to conventional methods. Especially, in situations involving high contrast between background and target, the proposed method has better reconstruction performance.

Acknowledgements

The authors thank Department of Applied Physics, University of Eastern Finland for providing the experimental data.

References

[1] J.G. Webster, Electrical Impedance Tomography, 1st ed., Bristol: Adam Hilger, 1990

[2] C.T. Crowe. *Multiphase Flow Handbook*. Boca Raton, FL: Taylor & Francis, 2006.

[3] G.F. Hewitt. Measurement of Two Phase Flow Parameters. London: Academic Press, 1978.

[4] T. Dyakowski, J. M. Hale, A. Jaworski, N. M. White, A. Nowakowski, G. Meng and S. Rwifa, "Dual-modality probe for characterization of heterogeneous Mixtures," IEEE Sensors Journal 5 134-138, 2005.

[5] S. Kim and A.K. Khambampati, "Mathematical concepts for image reconstruction in tomography," *Industrial Tomography: Systems and Applications,* 305, 2015.

[6] T. Dyakowski, "Process tomography applied to multi-phase flow measurement," Measurement Science and Technology 7 343–353, 1996.

[7] J. Chaouki, F. Larachi and M. P. Dudukovic, "Noninvasive tomographic and velocimetric monitoring of multiphase flows," Industrial and Engineering Chemistry Research 36 4476-4503, 2005.

[8] H.M. Prasser, "Novel experimental measuring techniques required to provide data for CFD validation," Nuclear Engineering and Design 238 744-770, 2008.

[9] R. A. Williams and X. Jia, "Tomographic imaging of particulate systems," Advanced Powder Technology 14 1-16, 2003.

[10] R. A. Williams and M. S. Beck (eds.) Process Tomography: Principles,Techniques and Applications. Oxford, UK: Butterworth-Heinemann 1995.

[11] H. McCann, D. M. Scott (eds.) 2005 *Process Imaging For Automatic Control*. Boca Raton, FL: CRC Press.

[12] D. Liu, A. K. Khambampati, S. Kim, and K. Y. Kim, "Multi-phase flow monitoring with electrical impedance tomography using level set based method," Nuclear Engineering and Design, vol. 289, pp. 108–116, 2015.

[13] B.S.Kim, D. Isaacson, H. Xia, T. J. Kao, J.C. Newell, and G.J. Saulnier, "A method for analyzing electrical impedance spectroscopy data from breast cancer patients," *Physiol. Meas.,* Vol. 28, pp. S237-246, 2007

[14] N.D. Harris, Applications of electrical impedance tomography in respiratory medicine PhD Thesis University of Sheffield, Sheffield, UK, 1991

[15] B.H. Brown, D.C. Barber, A.H. Morica, and A.D. Leathard, " Cardiac and respiratory related electric impedance changes in the human thorax," *IEEE Trans. Biomed. Eng.*, Vol. 41, pp. 729-734, 1994.

[16] J.M. Deibele, H. Luepschen, and S. Leonhardt, "Dynamic separation of pulmonary and cardiac changes in electrical impedance tomography," Physiol. Meas., Vol. 29, pp. S1-14, 2008

[17] T.J. Yorkey, J.G. Webster, and W.J. Tompkins, "Comparing reconstruction algorithms for electrical impedance tomography," *IEEE Trans. Biomed. Eng*., vol.34, pp. 843-852, 1987.

[18] A.Adler, T. Dai, and W.R.B. Lionheart, "Temporal image reconstruction in electrical impedance tomography," *Physiol. Meas*., vol.28, pp. S1-S11, 2007.

[19] W.Q. Yang, and L. Peng, "Image reconstruction algorithm for electrical capacitance tomography," *Meas. Sci. Technol*., vol.14, pp.1-13, 2003.

[20] A. Lipponen, A. Seppanen and J. Kaipio, "Electrical impedance tomography imaging with reduced-order model based on proper orthogonal decomposition" *J. Electron. Imag*., vol. 22 no. 2 pp. 023 008 2013.

[21] V. Kolehmainen, M. Lassas and P. Ola, "The Inverse Conductivity Problem with an Imperfectly Known Boundary." SIAM Journal on Applied Mathematics, vol. 66, no. 2, pp. 365–383, 2005.

[22] D. Liu, V. Kolehmainen, S. Siltanen and A. Seppanen, "Estimation of conductivity changes in a region of interest with electrical impedance tomography," *Inverse Problems Imag*., vol. 9, no. 1, pp. 211–229, 2015.

[23] D. Liu, V. Kolehmainen, S. Silatanen, A. Seppanen, "A nonlinear approach to difference imaging in EIT; Assessment of the robustness in the presence of modelling errors" *Inverse Problems*, vol. 31 no. 3 pp. 035012 2015.

[24] N. Otsu, "A threshold selection method from gray-level histograms," *IEEE Transactions on Systems, Man, and Cybernetics*;*SMC, vol.9, pp. 62-68, 1979.*

[25]B.S. Kim, A.K. Khambampati, S. Kim and K.Y. Kim, "Image reconstruction with an adaptive threshold technique in electrical resistance tomography," Measurement Science and Technology, Vol. 22, pp. 1-12, 2011.

[26] B.S. Kim, A.K. Khambampati, Y.J. Hong, S. Kim and K.Y. Kim, "Multiphase flow imaging using an adaptive multi-threshold technique in electrical resistance tomography," Flow measurement and Instrumentation, vol. 31, pp.25-34, 2013.

[27] K. S. Cheng, D. Isaacson, J. C. Newell, and D. G. Gisser, "Electrode models for electric current computed tomography," Biomedical Engineering, IEEE Transactions on, vol. 36, no. 9, pp. 918–924, 1989.

[28] M. Vauhkonen, D. Vadasz, P. A. Karjalainen, E. Somersalo, and J. P. Kaipio, "Tikhonov regularization and prior information in electrical impedance tomography," IEEE transactions on medical imaging, vol. 17, no. 2, pp. 285–293, 1998.

[29] P. Hua, J. G. Webster, W. J. Tompkins, "A regularised electrical impedance tomography reconstruction algorithm," Clin Phys Physiol Meas, vol. 9, pp. 137-41, 1998.

[30] L. M. Heikkinen, M. Vauhkonen, T. Savolainen, K. Leinonen, J. P. Kaipio, "Electrical process tomography with known internal structures and resistivities," Inverse Problems in Engineering, vol. 9, pp. 431-54, 2001.

[31] G. González, J. M. Huttunen, V. Kolehmainen, A. Seppänen and M. Vauhkonen, "Experimental evaluation of 3D electrical impedance tomography with total variation prior," Inverse Problems in Science and Engineering, vol. 24, no. 8, pp. 1411-1431, 2016.

[32] J. Kourunen, T. Savolainen, A. Lehikoinen, M. Vauhkonen and L. Heikkinen, " Suitability of a pxi platform for an electrical impedance tomography system," Measurement Science and Technology, vol. 20, 015503, 2009.

[33] L.M. Heikkinen, T. Vilhunen, R.M. West and M. Vaukonen, "Simultaneous reconstruction of electrode contact impedances and internal electrical properties: II. Laboratory experiments," Measurement Science and Technology, Vol. 13, 1855